High-Resolution Solid-State NMR Studies on Uniformly [^{13}C,^{15}N]-Labeled Ubiquitin

Karsten Seidel, Manuel Etzkorn, Henrike Heise, Stefan Becker, and Marc Baldus*[a]

Understanding of the effects of intermolecular interactions, molecular dynamics, and sample preparation on high-resolution magic-angle spinning NMR data is currently limited. Using the example of a uniformly [^{13}C,^{15}N]-labeled sample of ubiquitin, we discuss solid-state NMR methods tailored to the construction of 3D molecular structure and study the influence of solid-phase protein preparation on solid-state NMR spectra. A comparative analysis of $^{13}C'$, $^{13}C\alpha$, and $^{13}C\beta$ resonance frequencies suggests that ^{13}C chemical-shift variations are most likely to occur in protein regions that exhibit an enhanced degree of molecular mobility. Our results can be refined by additional solid-state NMR techniques and serve as a reference for ongoing efforts to characterize the structure and dynamics of (membrane) proteins, protein complexes, and other biomolecules by high-resolution solid-state NMR.

Introduction

Significant progress has recently been made in the use of magic-angle spinning (MAS[1]) NMR for structural studies in large, noncrystalline complexes. Structural models have been obtained, for example, for polypeptides that form macromolecular assemblies[2,3] or bind to large membrane proteins.[4] If 3D molecular structures are available as a reference, MAS-based solid-state techniques can be used to gain insight into the details of protein functioning, as demonstrated by several groups in the case of rhodopsin.[5] In addition, polypeptides and globular proteins have been an important target area of solid-state NMR, including studies on protein dynamics,[6,7] folding,[8,9] or ligand binding.[10] Whenever high-resolution X-ray or solution-state NMR 3D structures are available, globular proteins also represent a useful tool with which to develop and optimize solid-state NMR methodology and instrumentation. Such efforts have given rise to a handful of 3D structures ranging from two- and three-residue peptides to small proteins.[3,11–13] In particular, we have shown[13–15] that 3D molecular structures can be constructed through the use of a single, uniformly labeled sample.

Researchers have for a long time been interested in establishing a relationship between (supra)molecular structure and variations in solid-state NMR resonance frequencies, in contexts such as the polymorphism observed for compounds of low molecular weight.[16] In addition to variations in experimental conditions, such as hydration level or temperature,[7] details of sample preparation have been shown to affect MAS NMR spectra of microcrystalline proteins,[8,17] protein fibrils formed by β-amyloid peptides,[18] and α-synuclein (H.H., W. Hoyer, S.B., O. C. Andronesi, D. Riedel, M.B., unpublished results) and they can also play a significant role in the case of peptides and proteins reconstituted into lipid bilayers. While it is well known that hydration,[19,20] crystallization,[7,21,22] or the addition of cryoprotectants[23] can improve the spectral resolution of globular proteins, a detailed understanding of the relationship between solid-phase protein preparation and 3D molecular structure derived from MAS NMR is currently lacking. Such aspects have been thoroughly investigated by solution-state NMR in the case of ubiquitin, a 76-residue protein rich in secondary structure and involved in a variety of important cellular functions.[24] As well as the 3D structure[25] (PDB code: 1D3Z), folding intermediates[26] and, in particular, protein dynamics (see, for example, refs. [26–28]) have been examined in great detail.

Not surprisingly, ubiquitin has also become an attractive model system for MAS-based solid-state NMR studies, and yields MAS-NMR spectra that vary depending on the details of sample preparation.[17,20,22,29–32] Here we first derive sequential resonance assignments for uniformly labeled U-[^{13}C,^{15}N] ubiquitin precipitated from poly(ethylene glycol) (PEG). We show how (^{15}N, ^{15}N) correlations and indirectly detected proton–proton contacts can be used to monitor protein structure. Our experimental results show that the single-crystal structure of ubiquitin and the 3D structure in PEG-microcrystals must be closely related, and so we can compare our experimental findings with MAS-NMR results obtained on hydrated ubiquitin and precipitants obtained by use of 2-methylpentane-2,4-diol (MPD)[22] in close reference to the X-ray structure and solution-state NMR data. We conclude that the influence of sample preparation on 3D protein structure determination in solids is

[a] *K. Seidel,[+] M. Etzkorn,[+] Dr. H. Heise, Dr. S. Becker, Dr. M. Baldus*
Department of NMR-Based Structural Biology
Max Planck Institute for Biophysical Chemistry
37077 Göttingen (Germany)
Fax:(+49) 551-201-2202
E-mail: maba@mpibpc.mpg.de
[+] *These authors contributed equally to this work.*

Supporting information for this article is available on the WWW under http://www.chembiochem.org or from the author.

  DOI: 10.1002/cbic.200500085

most critical for molecular segments that exhibit a high degree of molecular mobility.

Results and Discussion

Structural characterization of UBI-P

Resonance assignments: To obtain sequential resonance assignments of UBI-P (precipitation with PEG) we used a set of two- and three-dimensional NC and CC correlation experiments. As an example, Figure 1 shows the results of a two-dimensional (^{13}C,^{13}C) spin-diffusion (SD[33]) experiment conducted under weak coupling conditions[34] on UBI-P for two different mixing times. For short mixing times ($t_{CC}=4$ ms; insert), only intraresidue correlations are visible, whilst for a mixing time of 100 ms, interresidue (^{13}C,^{13}C) correlations appear. These interactions are particularly easy to identify in the spectral region between 70 and 40 ppm, where intraresidue correlations are only possible for Ser, Thr, or Pro residues. In Figure 1, (i, $i\pm1$) and (i, $i\pm2$) correlations involving residues 1–4 and 17–27 are indicated as an example. To separate signal sets in an additional dimension, N–C-type correlation experiments[35] were conducted by use of SPECIFIC CP[36] transfers and SD (^{13}C,^{13}C) mixing blocks. Notably, no qualitative differences were detected in any of our spectra if this mixing unit was replaced by a DARR-type[37] irradiation scheme in which heteronuclear dipolar interactions involving protons and through-space proton–proton interactions are active.

Figure 2 shows an NCA-type spectrum obtained on UBI-P with an 800 MHz instrument. Additional experiments using variable ^{1}H decoupling strength reveal that the detected ^{15}N line width (0.8 ppm) is sensitive to the ^{1}H r.f. decoupling field strength in the 70–95 kHz range. Analysis of a series of CC and NC two- and three-dimensional spectra resulted in the de novo assignment of 86% of the 76 protein residues. The assignments are given as Supporting Information and reveal

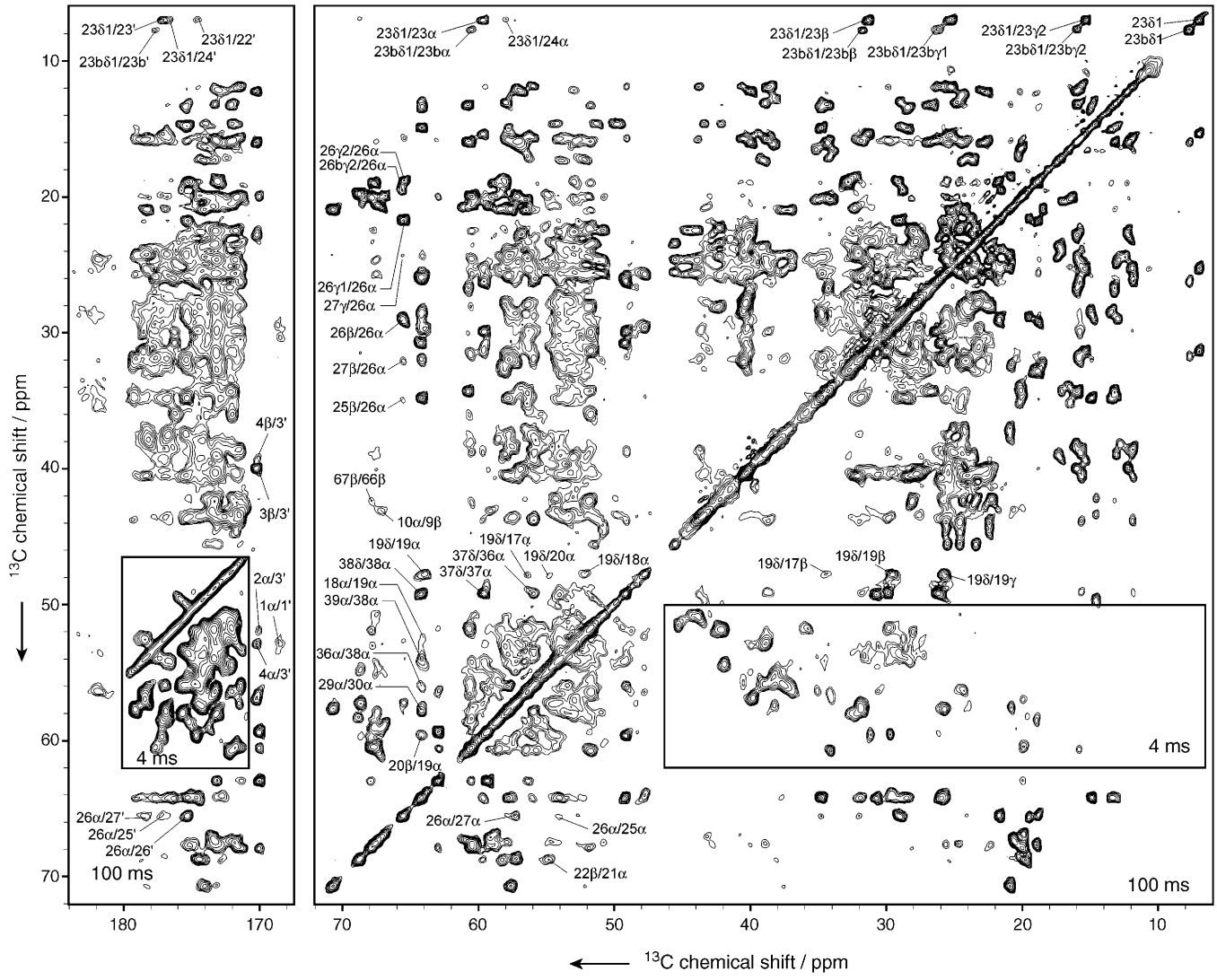

Figure 1. CC correlation spectrum obtained on U[^{13}C,^{15}N] UBI-P for mixing times of 100 ms and 4 ms (inserts) under weak coupling conditions.[34] Spectra were taken at 18.8 T B_0 field, 12.5 kHz MAS rate, and a temperature of 261 K. Signals were acquired over 36 h, with a maximum t_1 evolution time of 6.2 ms. Several (i, $i\pm1$) and (i, $i\pm2$) correlations are indicated as an example.

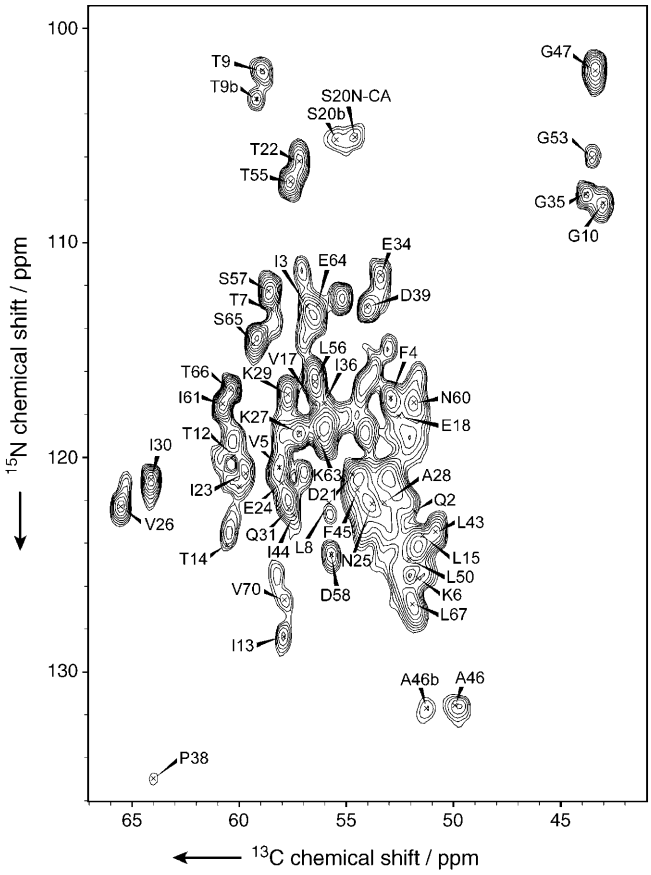

Figure 2. NCA correlation spectrum under experimental conditions as in Figure 1 with SPINAL-64 proton decoupling at 93 kHz r.f. field strength. The duration of the experiment was 2.3 h, with a maximum t_1 evolution time of 8 ms.

peak doubling for T9, I13, S20, I23, V26, P37, and A46. Two (C,C) correlation patterns are seen for Ile23 and V26 (Figure 1), for example, and two NCA peaks are found for T9 and S20 (Figure 2). Such peak doubling has been observed previously in (^{1}H,^{15}N) correlation spectra obtained on perdeuterated UBI-P samples[31] and for the catabolite repression histidine-containing phosphocarrier protein Crh,[8] and is indicative of the occurrence of multiple 3D conformations in the solid state. Notably, all sequential resonance assignments reported here are self-consistent and relate to the dominant peak intensities in the spectra.

Secondary structure analysis: As shown previously for selectively[38] or uniformly labeled[39] polypeptides, secondary chemical shifts provide a useful tool to describe protein secondary structure under MAS conditions. With the resonance assignments for UBI-P to hand, these parameters can be readily obtained by using the TALOS[40] software routine. Information about the backbone conformation in the solid state can also be obtained by correlating two anisotropic interactions such as the chemical-shift anisotropy (CSA) or the dipolar coupling in a two-dimensional experiment.[41] In uniformly labeled peptides, correlations between NH/NH[42] and NH/CH[43] dipolar tensors have been used for backbone dihedral angle determinations. Alternatively, relative tensor orientation may be encoded in the evolution of a double-quantum (2Q) two-spin state under the effect of two anisotropic interactions. Applications correlating CH/NH[44] and CN/CN[45] dipolar couplings or sequential carbonyl CSAs[46] have been demonstrated. In a 2Q correlation experiment under CN dipolar dephasing conditions, the signal amplitude can directly report on the backbone torsion angle and can hence conveniently be applied in multiply labeled polypeptides.[35] In the case of severe spectral overlap, extensions to three spectral dimensions are possible.[47]

Below we investigate two additional techniques used to refine the backbone topology in the context of a standard

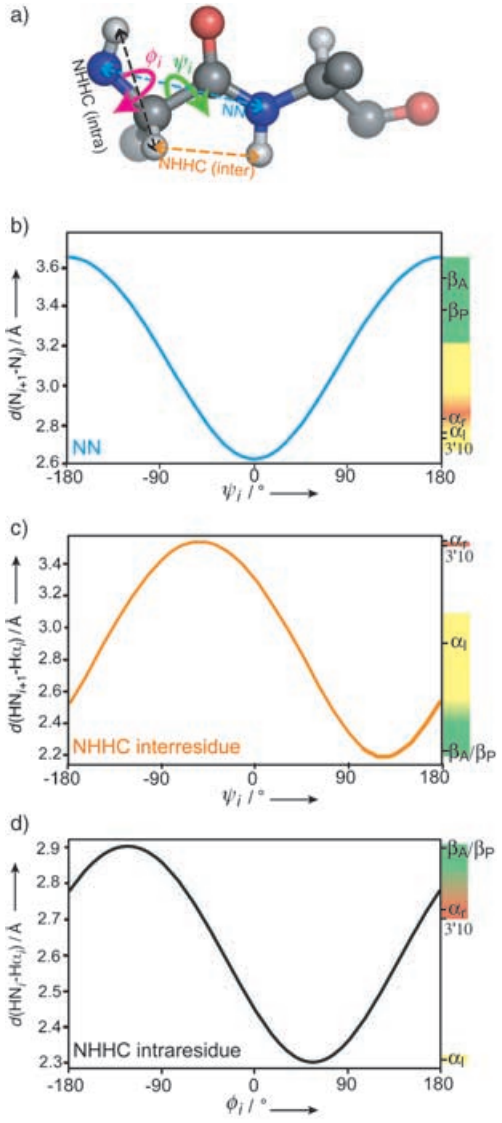

Figure 3. a) Molecular topology relevant in the context of NN and NHHC correlation experiments. B) Theoretical dependence of the N_i–N_{i+1} distance (blue) on the torsion angle ψ_i. C) and D) Relationships between the inter- (C, orange) and intraresidue (D, black) amide proton–Hα distance and the relevant torsion angles. Curves shown in C and D do not apply to Gly residues (see ref. [51] for further details). Colored regions added in B–D depict distances characteristic of L-α helix (yellow), R-α helix (red), and β-sheet regions (green).

(^{15}N,^{15}N) or (^{15}N,^{13}C) correlation experiment. As can be seen in Figure 3b, the (^{15}N,^{15}N) sequential distance is determined by the backbone torsion angle ψ, ranging from 2.6 Å to 3.65 Å. The corresponding dipolar couplings (see ref. [35] for a definition) take values between 68 Hz and 25 Hz, making the application of dipolar recoupling schemes in the presence of high-power proton decoupling difficult. Instead, (^{15}N,^{15}N) proton-driven spin diffusion experiments have been utilized in the context of solid-state NMR experiments under static[48] and MAS conditions.[12,42,49] Spectral spin diffusion[50] has been described by an exponential cross-peak buildup and a phenomenological spin-diffusion time constant T_{SD}. Here, T_{SD} is given by the (^{15}N,^{15}N) distance r_{12} of interest and the zero-quantum (0Q) line-shape function (J^{0Q}), evaluated at the isotropic chemical shift difference of ^{15}N spin 1 and 2 for a given MAS rate. In the case of proton–proton mixing, we have found[14] that $J^{0Q}(\omega_R)$ scales with $1/\omega_R^2$. To investigate whether a similar dependence is observed for (^{15}N,^{15}N) mixing, we conducted test experiments on U-[^{13}C,^{15}N]-labeled L-histidine·HCl. Figure 4a shows the $^{15}N_{\delta1}$–$^{15}N_{\varepsilon2}$ cross-peak intensity measured for two MAS rates as a function of the SD time t_{NN}. Both buildup curves were recorded at 9.4 T. Comparison to a theoretical description as in ref. [14] confirms that the zero-quantum line-shape function indeed scales with $1/\omega_R^2$ and that at a mixing time of 5 s and an MAS rate of 11 kHz, correlations should involve predominantly (^{15}N–^{15}N) distances below 3 Å (Figure 4b).

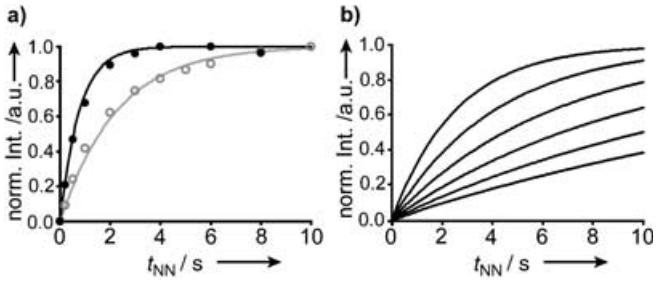

Figure 4. a) $^{15}N_{\delta1}$–$^{15}N_{\varepsilon2}$ cross-peak intensity measured on uniformly [^{13}C,^{15}N]-labeled L-histidine·HCl at $\omega_r = 7$ kHz (●) and $\omega_r = 12$ kHz (○). Both buildup curves were recorded at 9.4 T. Experimental results at 7 kHz were fitted (black line) by use of the theoretical model described in ref. [14] and rescaled with the square of the ratio between the two spinning speeds (see ref. [14]) to reproduce data obtained at 12 kHz (gray line). b) Theoretical cross-peak buildup behavior, predicted with the help of a) at $\omega_r = 11$ kHz for (^{15}N,^{15}N) distances of 2.4, 2.6, 2.8, 3.0, 3.2, and 3.4 Å from top to bottom.

The corresponding spectrum in the case of U-[^{13}C,^{15}N]-labeled UBI-P recorded at 14.1 T with a spinning speed of $\omega_r = 11$ kHz is shown in Figure 5. The experimental results are compared with predictions obtained from the known 3D (crystal) structure of ubiquitin and the chemical-shift assignments for UBI-P. Sequential contacts below 3 Å are indicated by filled circles. In line with Figure 3b, the vast majority of the observed correlations correspond to sequential (^{15}N,^{15}N) transfer in right-handed helices (underlined) and β-turn (dashed underlined) regions of the protein. Moreover, all correlations expected from β-sheet regions are in general weak or missing. Notably, correlations not identified in Figure 5 can largely be explained by missing ^{15}N assignments. We can hence conclude that (^{15}N–^{15}N) distances of or below 3 Å dominate the NN spectrum under the experimental conditions employed (MAS rate: 11 kHz, mixing time: 5 s, B_0: 600 MHz).

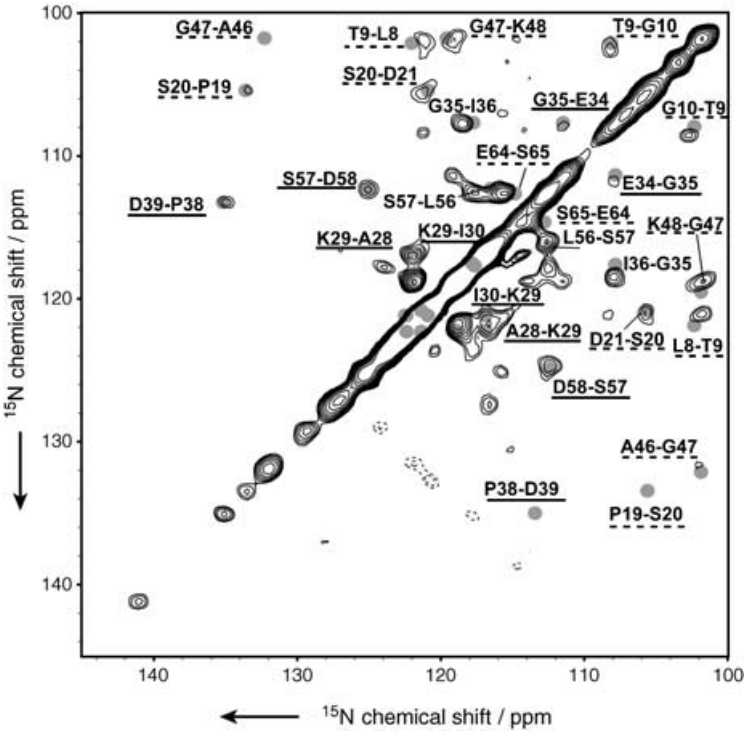

Figure 5. NN spin diffusion spectrum on UBI-P recorded at 14.1 T with a spinning speed of $\omega_r = 11$ kHz and $t_{NN} = 5$ s. The temperature was set to −14 °C and acquisition times of 15 ms in t_2 and 14 ms in t_1 were used. The total experiment time was approx. 15 h, with 64 scans per t_1 increment. Predicted N–N sequential contacts (with use of the X-ray structure as reference) below 3 Å are indicated by filled gray circles. Assignments are underlined if found in elements of defined secondary structure [helix (solid) and β-turns (dashed)]. Spinning side-band intensities are dotted.

As can be seen in Figure 3c and d, NH–HCα distances provide an additional, sensitive measure of the local backbone conformation. In particular, sequential NH–HCα distances in β-sheet regions are shorter than the corresponding intraresidue values. Figure 6 shows the (NH,Cα) region of an NHHC[14,30] experiment on UBI-P, that permits the recording of such interactions in a ^{15}N evolution and ^{13}C detection period. The experimental results are again compared to structural data classified into intraresidue and interresidue polarization transfer for amide proton–Hα distances up to 2.5 Å. As expected from earlier studies in small molecules,[14] mixing for 90 μs produces an NHHC spectrum in which proton–proton interactions of a length scale of 2–3 Å are dominant. Correspondingly, the spectrum shown in Figure 6 can be explained well by the dominant influence of interresidue correlations involving β-sheet regions of the protein. Complementary to the NN case, in which both α-helix and β-turn motifs appear in the spectrum, intraresidue NHHC correlations are predominantly

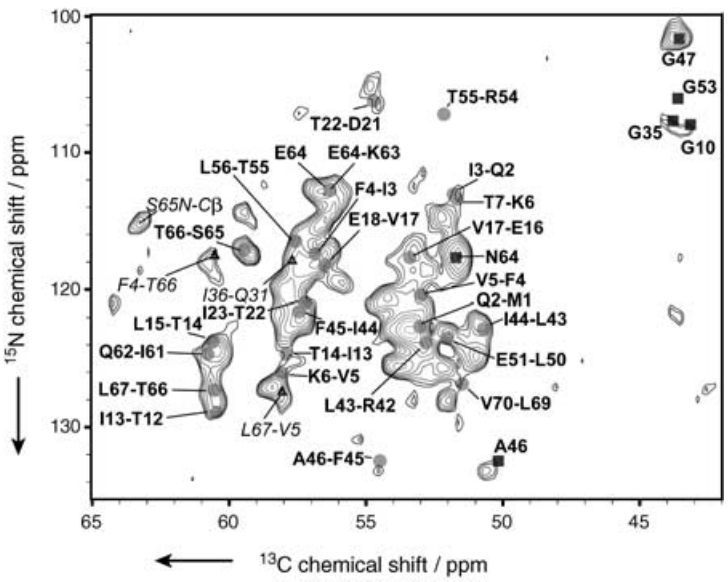

Figure 6. NHHC spectrum on UBI-P with a total number of 6080 scans per t_1 increment. Data were recorded at −14 °C at 14.1 T with a spinning speed of 11 kHz. Predictions for intra- [HN_i– $HC\alpha_i$] (squares) and interresidue [HN_{i+1}–$HC\alpha_i$] (circles) contacts below 2.5 Å are included. Triangles indicate short (< 2.7 Å) contacts between HN_i–$HC\alpha_i$ with $|j-i|>1$.

the result of β-turn conformations such as in the case of A46. For glycine, strong intraresidue NHHC correlations are also possible for other secondary structure elements. In the case of ubiquitin, these mainly relate to β-turn regions of the protein. In addition, the NHHC spectrum contains correlations involving intra- and interresidue NH–HCβ spin pairs that encode additional information about the torsion angle χ.[51] Finally, inter-β-strand NH–HCα correlations relating to F4 NH–T66 Hα and L67 NH–V5 Hα contacts are also detected. Notably, these distances (2.65 Å) belong to the shortest long-range contacts found in the X-ray structure. In two spectral dimensions, these correlations cannot be assigned unequivocally. As in Figure 5, correlations not identified in Figure 6 are the result of missing ^{15}N and ^{13}C resonance assignments. Spectral overlap can be greatly reduced by use of 3D spectroscopy,[52] however, and may provide long-range NHHC constraints useful in a subsequent structure calculation.

The results shown in Figures 3–6 demonstrate that NN and NHHC correlations can provide a complementary means to characterize protein secondary structure if recorded under appropriate experimental conditions. Together with TALOS-derived torsion-angle constraints (Figure 7, empty circles), these correlations can hence be used to increase the number of torsion-angle constraints. For UBI-P, torsion-angle predictions classified as reliable in TALOS are in good agreement with the X-ray structure ("×" symbols in Figure 7). The analysis of NN and NHHC spectra provides a total of 19 additional (φ,ψ) torsion-angle constraints (filled circles) that resolve ambiguities detected by TALOS and can be used in the context of a structure calculation. The corresponding residues are often found in loop regions of the protein, where TALOS predictions are known to be most unreliable. Only one (ψ_{54}) of the total of 92 refined torsion angles differs significantly from values expected from the X-ray structure. These results confirm that the secondary structures of UBI-P microcrystals agree with data obtained by X-ray crystallography and solution-state NMR.

Investigation of 3D structure: Figure 8 compares results of a (^{13}C,^{13}C) SD experiment (mixing time: 40 ms, MAS rate: 11 kHz, 600 MHz, blue) with CHHC[14,15,30] data (red) obtained for a proton–proton mixing time of 250 μs. There are notable differences between the two spectra, which are most pronounced in the Cα region. Most of these CHHC correlations cannot be assigned unequivocally by 2D spectroscopy. However, by assuming a homology model, we can compare our CHHC data to predictions from the X-ray structure and resonance assignments obtained for UBI-P considering (^1H,^1H) distances up to 3.5 Å. According to ref. [14], such interactions should dominate the CHHC spectrum under the experimental conditions consid-

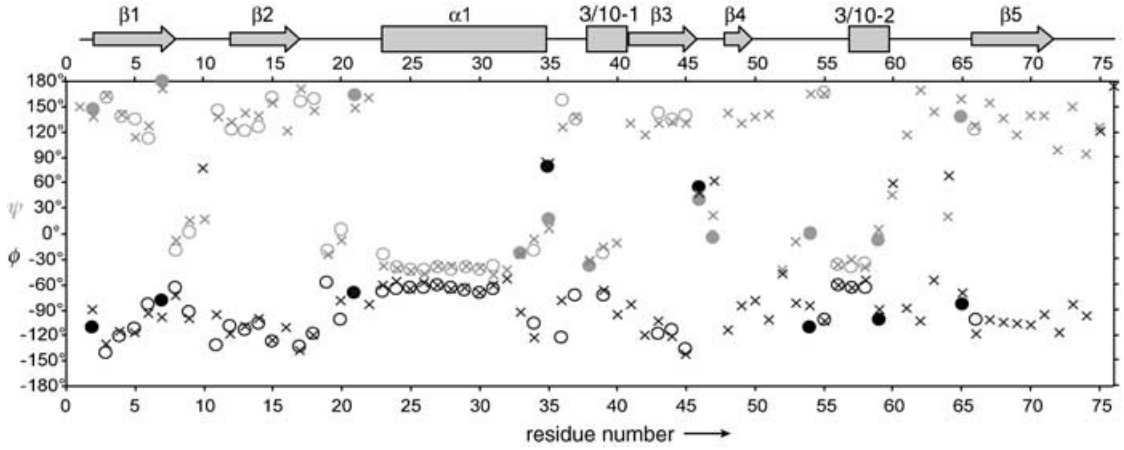

Figure 7. Comparison between dihedral angles as found in the crystal structure (X) with TALOS predictions (○). Ambiguities in the TALOS analysis can be resolved with the aid of NN and NHHC spectra, resulting in a total of 19 additional dihedral angles (●).

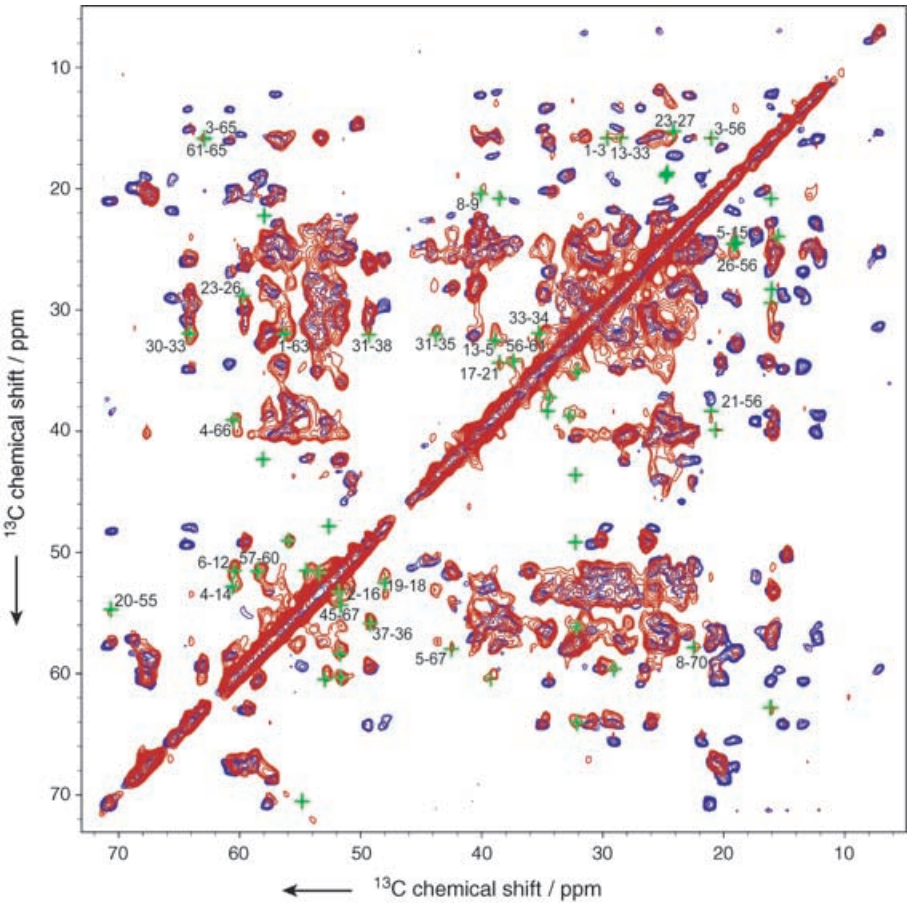

Figure 8. Comparison between a (^{13}C,^{13}C) SD experiment (mixing time: 40 ms, MAS rate 11 kHz, 600 MHz, blue) and a CHHC[14,15,30] spectrum (red) obtained for a proton–proton mixing time of 250 μs on UBI-P. CHHC correlations that do not overlap with SD cross-peaks and are consistent with short, medium, or long-range (X–Y) contacts between residues X and Y are indicated by green symbols.

ered here. Except for correlations involving methyl protons, which are attenuated due to the short CP time but appear for longer contact times, a variety of medium- and long-range contacts in the distance range under consideration can be identified. Correlations that do not overlap with intraresidue cross-peaks of the CC spectrum are indicated by green symbols. For example, (*i*, *i*+3) contacts such as 23–26 or 30–33 are observed for the central α-helix. In addition, long-range contacts such as 4–66 or 5–67, connecting β-strand 1 (β1) and β-strand 5 (β5), are readily found. Likewise, β-strands 1 and 2 are connected by CHHC correlations 6–12 and 4–14. In total, 30 CHHC constraints were identified, relating to four sequential, nine medium-range, and 17 long-range contacts. The number of unequivocal CHHC distance restraints could be increased by use of three-dimensional correlation spectroscopy[52] or CHHC data with different mixing times (data not shown). Moreover, iterative methods demonstrated in ref. [13] or implemented in software routines such as CYANA[53] or ARIA[54] could be used to resolve ambiguities in the CHHC assignment process.

We next investigated whether the CHHC constraints identified in Figure 8, together with torsion-angle constraints derived from a combined TALOS, NN, and NHHC structure analysis, would be sufficient to construct a 3D molecular structure through the use of CNS. This approach hence does not deliver a de novo 3D structure of UBI-P microcrystals, but makes comparison of MAS-based NMR data sets to existing structures possible. The resulting ensemble of ten structures selected according to the lowest overall energy and aligned along the backbone atoms of residues M1 to V70 with the aid of MOLMOL is shown in Figure 9. The overall fold and the characteristic secondary structure elements are reproduced well, suggesting that the X-ray structure and the 3D structure of PEG-precipitated ubiquitin must be closely related. When comparing the effect of sample preparation on solid-phase protein structure we will hence utilize X-ray and solution-state NMR results as a reference.

The effect of sample preparation

As we have previously demonstrated for Crh,[8] comparison of MAS-NMR derived resonance assignments to structural data obtained from other resources provides a useful instrument with which to study solid-phase protein structure. We begin by comparing (^{13}C,^{13}C) spectra of UBI-P (Figure 10, red) with results obtained on UBI-H (rehydrated, Figure 10c, green). While the detected ^{13}C line width is comparable, chemical shift variations for both backbone and side-chain resonances are visible. Backbone Cα and Cβ resonances for S20, F45, and T22, for example, vary between 1 ppm and over 2 ppm. Similar variations are also seen for C′–Cx ($x = \alpha,\beta$) correlations, as visible in Figure 10b. Figure 10a compares correlations found for UBI-H with resonance assignments reported for UBI-M[22] (precipitated with MPD). Interestingly, the agreement between NMR spectra for those two preparations is far better than that between microcrystals prepared from PEG and MPD. We hence conclude that hydrated ubiquitin adopts a solid-phase (supra)molecular structure that closely resembles that present in the case of MPD precipitants. Chemical-shift assignments of UBI-M have already been compared in ref. [22] with solution-state NMR data reported by Wand and co-workers,[55] and these resonance assignments are in good agreement with values reported by Bax and co-workers.[56] In Figure 11, the last set of values has been subtracted from chemical-shift assignments obtained for UBI-P. For the sake of

Figure 9. Ensemble of 10 UBI-P structures calculated by use of CNS consistent with TALOS, NN, NHHC, and CHHC data. Structures were aligned along the backbone atoms of residues M1 to V70 with the aid of MOLMOL.

clarity, chemical-shift changes are plotted only for C′, Cα, and Cβ. For many residues, these variations are significantly larger than the natural line width (ca. 0.5 ppm). At the N terminus, the strongest variations are observed for residues 1 and 2 at the beginning of the first β-strand and, subsequently, within the loop connecting β-strand 2 and the central α-helix. Interestingly, both regions exhibit a high degree of molecular motion when analyzed in weakly aligned, solubilized protein samples.[28] In the α-helix α1, strong variations are found for residues 23 and 25, which have been shown to exhibit conformational exchange in solution.[27,57] Such a mechanism[27] could also explain the large variations seen for Glu18. With the exception of residue 33, chemical shift variations are small for α-helical residues 26–34, again in agreement with a recent solution-state NMR study on protein dynamics.[28] An accurate analysis for residues 40–50 is difficult, due to missing solid-state NMR assignments for residues 40, 41 and 49. Strong variations are again observed for the 3/10-helix 57–59, in agreement with ref. [28]. Finally, order parameters close to the 0 reported for the C terminus in the solution state are consistent with a highly flexible protein C-terminal segment in UBI-P, which gives rise to a strong reduction of (^{1}H,^{13}C) and (^{1}H,^{15}N) CP efficiency. These residues are missing in the CC and NC spectra for the experimental temperatures used in our study; this would be consistent with molecular mobility that gives rise to

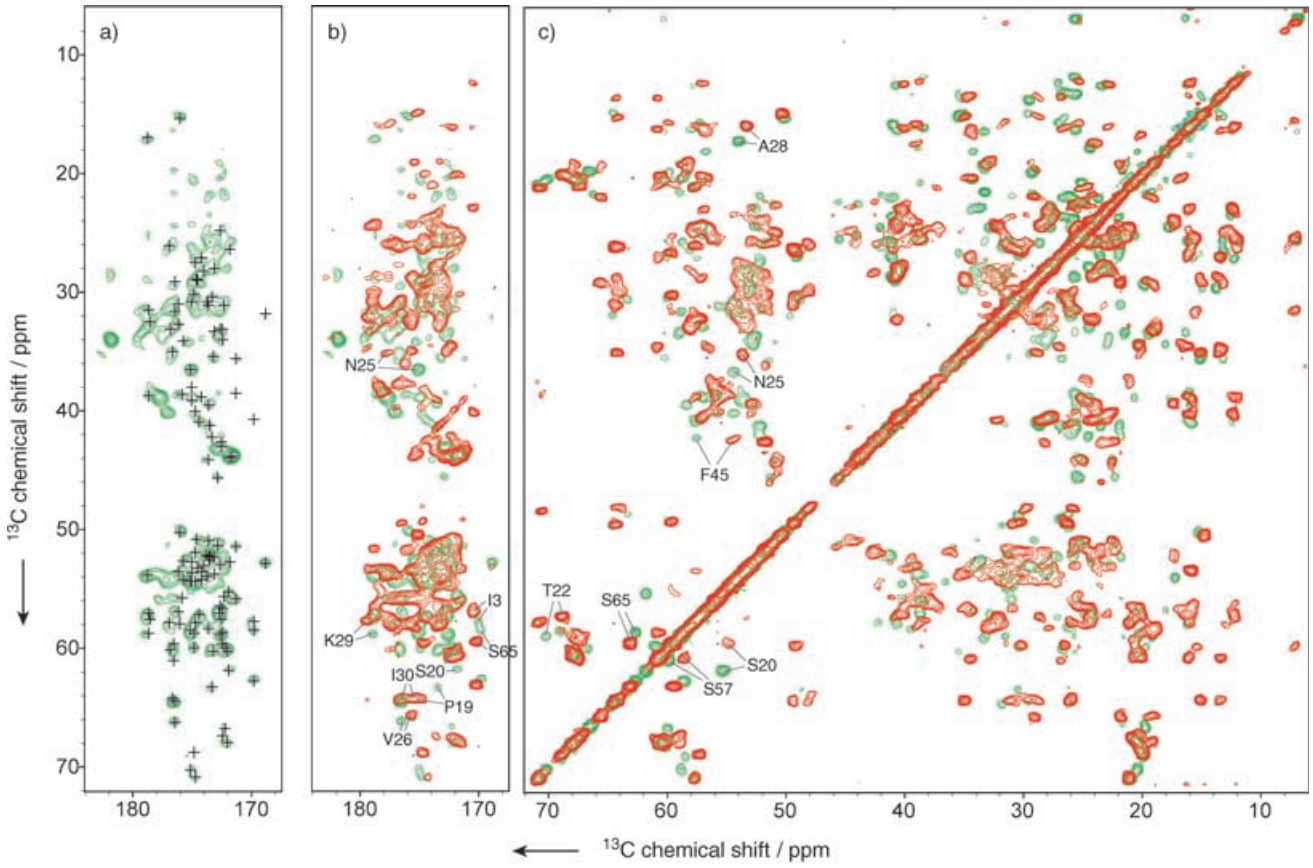

Figure 10. Comparison of (^{13}C,^{13}C) SD spectra for UBI-P (red) with experimental results obtained on UBI-H (green) with an SD mixing time of 40 ms SD and an MAS rate of 11 kHz at 600 MHz.

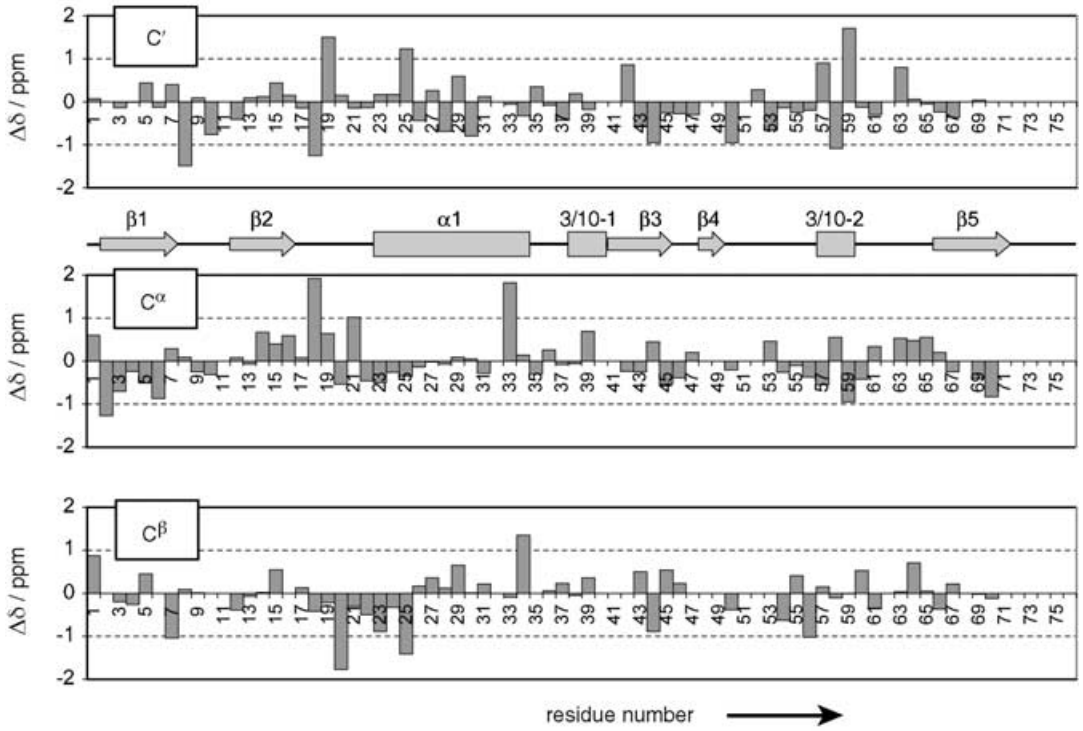

Figure 11. Difference between resonance assignments obtained for UBI-P and solution-state NMR shifts as reported by Wang et al.[56]

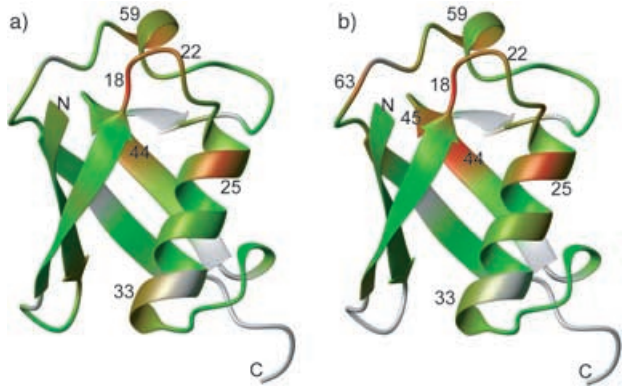

Figure 12. Chemical shift difference between: a) UBI-P and solution-state NMR,[56] and b) UBI-P and UBI-M,[22] shown on the 3D (crystal) structure of ubiquitin. The added norm of C′, Cα, and Cβ chemical shift variations is plotted, ranging from small (green, 0 ppm) to large (red, 3.6 ppm in (a), 4.7 ppm in (b)) values. Residues unassigned in at least one of the compared data sets are indicated in gray.

a reduction of through-space couplings and is only frozen out at lower temperatures.

In Figure 12a, we display the chemical shift changes shown in Figure 11 on the 3D (crystal) structure of ubiquitin. For simplicity, only the added norm of C′, Cα, and Cβ chemical shift variations is plotted, ranging from small (green) to large (red) values. Unassigned residues are indicated in gray. With the exception of α-helical residues known to undergo conformational exchange and the C terminus, the largest chemical variations are observed for the loop comprising residues 16–22 and the small 3/10-helix 57–59, which are found in close spatial proximity in the 3D structure. In contrast with changes at the end of α-helix 1, these variations could hence speak in favor of structural differences between solution and solid-state conformation, due to increased molecular mobility. If this conclusion were correct, similar protein regions should be affected if protein microcrystals were prepared with use of MPD instead of PEG. Correspondingly, Figure 12b encodes chemical shift variations between UBI-P assigned in this study and resonance assignments on UBI-M as reported in ref. [22]. Indeed, many protein segments identified in Figure 12a also reveal strong chemical shift variations between UBI-P and UBI-M. In addition, substantial chemical shift changes are seen for F45 and K63. The reason for these variations can possibly be further elucidated by measuring site-resolved chemical shielding anisotropies, T_1, T_2, and $T_{1\rho}$ relaxation rates, or dipolar order parameters under MAS conditions.

Conclusion

We have applied a series of correlation experiments to study the effect of sample preparation on a globular, solid-phase protein. The 3D molecular structure was studied by using a single U-[^{13}C,^{15}N]-labeled sample of ubiquitin, and chemical-shift variations were evaluated in reference to solution-state NMR data. Our comparative study of ^{13}C′, ^{13}Cα, and ^{13}Cβ resonance frequencies suggests that ^{13}C chemical-shift variations are most likely to occur in protein regions that exhibit an enhanced degree of molecular mobility. Complementary information on molecular dynamics may be obtainable from a residue-specific analysis of ^{13}C and ^{15}N chemical-shielding anisotropies,

^{1}H and ^{15}N resonance frequencies, T_1, T_2, and $T_{1\rho}$ relaxation rates, or CH and CC order parameters.[15] The design and application of these techniques in well characterized proteins such as ubiquitin provides a useful reference for future studies of molecular structure and dynamics in (membrane) proteins of unknown structure by high-resolution solid-state NMR.

Experimental Section

Sample preparation: A U-[^{13}C,^{15}N]-labeled sample of L-histidine·HCl was obtained from Cambridge Isotope Laboratories (CIL, Andover, MA). Uniformly [^{13}C,^{15}N]-labeled ubiquitin was purchased from VLI research (Malvern, PA) or expressed recombinantly in *Escherichia coli* and purified by established procedures.[58] After freeze-drying, two alternative routes of sample preparation were followed. As described in refs. [8, 17], ubiquitin (8 mg) was precipitated from poly(ethylene glycol) (PEG) and transferred into a 4 mm MAS rotor. Additional experiments were conducted on U-[^{13}C,^{15}N]-ubiquitin (6 mg) that was hydrated with H_2O (10 μL) after lyophilization in the rotor. For brevity, ubiquitin sample preparations relevant in the context of this study are described by UBI-P (PEG precipitation), UBI-H (rehydrated), and UBI-M (MPD precipitated). While experimental results are shown for UBI-P and UBI-H, resonance assignments for UBI-M were taken from refs. [22, 32].

Solid-state NMR experiments: All NMR experiments were conducted with use of 4 mm triple-resonance (^{1}H,^{13}C,^{15}N) probeheads at a static magnetic field of 18.8 T and 14.1 T corresponding to 800 MHz and 600 MHz proton resonance frequencies (Bruker Biospin, Karlsruhe, Germany), respectively. Hartmann–Hahn[59] (^{1}H,^{13}C) and (^{1}H,^{15}N) cross polarization was established by use of ramped[60] radio frequency (r.f.) fields. For proton decoupling, TPPM[61] and SPINAL-64[62] multiple-pulse schemes were used. Sequential resonance assignments were obtained from combining results of two- and three-dimensional (^{15}N,^{13}C) correlation experiments as described in refs. [35, 36] with results of (^{13}C,^{13}C) correlation experiments performed under weak coupling conditions.[34] MAS rates between 9 and 12.5 kHz were employed at sample temperatures between −14 °C and −5 °C. C/NHHC correlation experiments were conducted as described in refs. [14, 30] with use of HH mixing times between 90 μs and 400 μs, bracketed by short (^{1}H,X) CP transfers for contact times of 80–110 μs (X = ^{13}C) and 200 μs (X = ^{15}N).

Solid-state NMR data analysis: All spectra were processed by use of QSINE window functions in F1 and F2 and analyzed with the aid of Sparky version 3.110 (T. D. Goddard, D. G. Kneller, University of California). Resonance assignments were evaluated by using TALOS version 2003.027.13.05,[40] which predicts the backbone dihedral angles φ and ψ on the basis of chemical shift and sequence homology with proteins of known structure and assigned (solution-state) chemical shifts. As explained in the main text, results of NN and NHHC data were used to resolve ambiguities for dihedral angle pairs not classified as reliable (i.e., "good") in TALOS. For cross validation, the crystal structure[63] (PDB code: 1UBQ) was used.

Structure calculation: Structure calculations were performed by use of a simulated annealing protocol in CNS[64] version 1.1 with the PROTEIN-ALLHDG[65] parameter file. Backbone angles predicted by TALOS, using chemical-shift assignments for N, C′, Cα, and Cβ, were refined by an analysis of NN and NHHC spectra as described below. In total, 45 φ angles and 47 ψ angles were used in the simulation. Restraints were enforced by square-well potentials with no energy contribution for deviations within the predicted RMSD. Likewise, constraints for proton–proton distances were invoked with an allowed upper limit of 3.5 Å and no lower bounds. Simulations started from an extended conformation generated from the amino acid sequence. The structure calculation protocol consisted of three stages: 1) high-temperature annealing in torsion-angle space, in 2000 time steps of 0.015 ps at 50 000 K, 2) slow-cool annealing in torsion-angle space, in 4000 steps of 0.015 ps, and temperature reduction from 50 000 K to zero in steps of 250 K, and 3) final conjugate gradient minimization in 20 cycles of 100 steps each. Force constants were set to 300, 300, and 150 kcal mol^{-1} Å^{-2} for the distance restraints, and 100, 200, and 400 kcal mol^{-1} rad^{-2} for the backbone angle restraints during the three stages. Ambiguities in the assignments of methylene and methyl protons were accounted for by R^{-6} averaging over all possible contacts. A set of 100 structures was calculated, starting with different initial velocities. An ensemble of ten structures was selected according to the lowest overall energy, and was aligned along the backbone atoms of residues M1 to V70 by use of MOLMOL 2K.2.[66]

Acknowledgements

We thank Dr. Sorin Luca, Brigitta Angerstein, and Adam Lange for help during various stages of this research project. Scientific discussions with Professor C. Griesinger are gratefully acknowledged. This work was funded in part by the MPG and a Liebig fellowship from the Fonds der Chemischen Industrie to H.H.

Keywords: magic-angle spinning · molecular dynamics · NMR spectroscopy · solid state · structure elucidation · ubiquitin

[1] E. R. Andrew, A. Bradbury, R. G. Eades, *Nature* **1958**, *182*, 1659.
[2] A. T. Petkova, Y. Ishii, J. J. Balbach, O. N. Antzutkin, R. D. Leapman, F. Delaglio, R. Tycko, *Proc. Natl. Acad. Sci. USA* **2002**, *99*, 16742–16747; R. A. Kammerer, D. Kostrewa, J. Zurdo, A. Detken, C. Garcia-Echeverria, J. D. Green, S. A. Muller, B. H. Meier, F. K. Winkler, C. M. Dobson, M. O. Steinmetz, *Proc. Natl. Acad. Sci. USA* **2004**, *101*, 4435–4440.
[3] C. P. Jaroniec, C. E. MacPhee, V. S. Bajaj, M. T. McMahon, C. M. Dobson, R. G. Griffin, *Proc. Natl. Acad. Sci. USA* **2004**, *101*, 711–716.
[4] S. Luca, J. F. White, A. K. Sohal, D. V. Filippov, J. H. van Boom, R. Grisshammer, M. Baldus, *Proc. Natl. Acad. Sci. USA* **2003**, *100*, 10706–10711.
[5] G. Grobner, I. J. Burnett, C. Glaubitz, G. Choi, A. J. Mason, A. Watts, *Nature* **2000**, *405*, 810–813; A. F. L. Creemers, S. Kiihne, P. H. M. Bovee-Geurts, W. J. DeGrip, J. Lugtenburg, H. J. M. de Groot, *Proc. Natl. Acad. Sci. USA* **2002**, *99*, 9101–9106; A. B. Patel, E. Crocker, M. Eilers, A. Hirshfeld, M. Sheves, S. O. Smith, *Proc. Natl. Acad. Sci. USA* **2004**, *101*, 10048–10053.
[6] D. A. Torchia, *Annu. Rev. Biophys. Bioeng.* **1984**, *13*, 125–144; N. Giraud, A. Böckmann, A. Lesage, F. Penin, M. Blackledge, L. Emsley, *J. Am. Chem. Soc.* **2004**, *126*, 11422–11423.
[7] H. B. R. Cole, D. A. Torchia, *Chem. Phys.* **1991**, *158*, 271–281.
[8] A. Böckmann, A. Lange, A. Galinier, S. Luca, N. Giraud, H. Heise, M. Juy, R. Montserret, F. Penin, M. Baldus, *J. Biomol. NMR* **2003**, *27*, 323–339.
[9] M. Etzkorn, A. Böckmann, A. Lange, M. Baldus, *J. Am. Chem. Soc.* **2004**, *126*, 14746–14751; H. Heise, S. Luca, B. de Groot, H. Grubmüller, M. Baldus, *Biophys. J.* **2005**, in press; R. H. Havlin, R. Tycko, *Proc. Natl. Acad. Sci. USA* **2005**, *102*, 3284–3289.
[10] S. G. Zech, E. Olejniczak, P. Hajduk, J. Mack, A. E. McDermot, *J. Am. Chem. Soc.* **2004**, *126*, 13948–13953.
[11] K. Nomura, K. Takegoshi, T. Terao, K. Uchida, M. Kainosho, *J. Am. Chem. Soc.* **1999**, *121*, 4064–4065; C. M. Rienstra, L. Tucker-Kellogg, C. P. Jaroniec, M. Hohwy, B. Reif, M. T. McMahon, B. Tidor, T. Lozano-Perez, R. G. Griffin, *Proc. Natl. Acad. Sci. USA* **2002**, *99*, 10260–10265.
[12] F. Castellani, B. van Rossum, A. Diehl, M. Schubert, K. Rehbein, H. Oschkinat, *Nature* **2002**, *420*, 98–102.

[13] A. Lange, S. Becker, K. Seidel, O. Pongs, M. Baldus, *Angew. Chem.* **2005**, *117*, 2125 – 2129; *Angew. Chem. Int. Ed.* **2005**, *44*, 2089 – 2092.
[14] A. Lange, K. Seidel, L. Verdier, S. Luca, M. Baldus, *J. Am. Chem. Soc.* **2003**, *125*, 12640 – 12648.
[15] K. Seidel, M. Etzkorn, L. Sonnenberg, C. Griesinger, A. Sebald, M. Baldus, *J. Phys. Chem. A* **2005**, *109*, 2436 – 2442.
[16] R. K. Harris in *Encyclopedia of Nuclear Magnetic Resonance* (Eds. D. M. Grant, R. K. Harris), Wiley, Chichester, **1996**, pp. 3734 – 3740.
[17] R. W. Martin, K. W. Zilm, *J. Magn. Reson.* **2003**, *165*, 162 – 174.
[18] A. T. Petkova, R. D. Leapman, Z. Guo, W.-M. Yau, M. P. Mattson, R. Tycko, *Science* **2005**, *307*, 262 – 265.
[19] R. B. Gregory, M. Gangoda, R. K. Gilpin, W. Su, *Biopolymers* **1993**, *33*, 513 – 519.
[20] M. Hong, *J. Magn. Reson.* **1999**, *139*, 389 – 401; S. Luca, M. Baldus, *J. Magn. Reson.* **2002**, *159*, 243 – 249.
[21] S. O. Smith, S. Farrjones, R. G. Griffin, W. W. Bachovchin, *Science* **1989**, *244*, 961 – 964; J. Pauli, B. van Rossum, H. Forster, H. J. M. de Groot, H. Oschkinat, *J. Magn. Reson.* **2000**, *143*, 411 – 416; A. McDermott, T. Polenova, A. Bockmann, K. W. Zilm, E. K. Paulsen, R. W. Martin, G. T. Montelione, *J. Biomol. NMR* **2000**, *16*, 209 – 219.
[22] T. I. Igumenova, A. E. McDermott, K. W. Zilm, R. W. Martin, E. K. Paulson, A. J. Wand, *J. Am. Chem. Soc.* **2004**, *126*, 6720 – 6727.
[23] D. L. Jakeman, D. J. Mitchell, W. A. Shuttleworth, J. N. S. Evans, *J. Biomol. NMR* **1998**, *12*, 417 – 421.
[24] J. Marx, *Science* **2002**, *297*, 1792 – 1794.
[25] G. Cornilescu, J. L. Marquardt, M. Ottiger, A. Bax, *J. Am. Chem. Soc.* **1998**, *120*, 6836 – 6837.
[26] B. Brutscher, R. Bruschweiler, R. R. Ernst, *Biochemistry* **1997**, *36*, 13043 – 13053.
[27] N. Tjandra, S. E. Feller, R. W. Pastor, A. Bax, *J. Am. Chem. Soc.* **1995**, *117*, 12562 – 12566.
[28] W. Peti, J. Meiler, R. Bruschweiler, C. Griesinger, *J. Am. Chem. Soc.* **2002**, *124*, 5822 – 5833.
[29] S. K. Straus, T. Bremi, R. R. Ernst, *J. Biomol. NMR* **1998**, *12*, 39 – 50.
[30] A. Lange, S. Luca, M. Baldus, *J. Am. Chem. Soc.* **2002**, *124*, 9704 – 9705.
[31] E. K. Paulson, C. R. Morcombe, V. Gaponenko, B. Dancheck, R. A. Byrd, K. W. Zilm, *J. Am. Chem. Soc.* **2003**, *125*, 15831 – 15836.
[32] T. I. Igumenova, A. J. Wand, A. E. McDermott, *J. Am. Chem. Soc.* **2004**, *126*, 5323 – 5331.
[33] N. Bloembergen, *Physica* **1949**, *15*, 386 – 426.
[34] K. Seidel, A. Lange, S. Becker, C. E. Hughes, H. Heise, M. Baldus, *Phys. Chem. Chem. Phys.* **2004**, *6*, 5090 – 5093.
[35] M. Baldus, *Prog. Nucl. Magn. Reson. Spectrosc.* **2002**, *41*, 1 – 47.
[36] M. Baldus, A. T. Petkova, J. Herzfeld, R. G. Griffin, *Mol. Phys.* **1998**, *95*, 1197 – 1207.
[37] K. Takegoshi, S. Nakamura, T. Terao, *Chem. Phys. Lett.* **2001**, *344*, 631 – 637.
[38] H. Saito, *Magn. Reson. Chem.* **1986**, *24*, 835 – 852.
[39] S. Luca, D. V. Filippov, J. H. van Boom, H. Oschkinat, H. J. M. de Groot, M. Baldus, *J. Biomol. NMR* **2001**, *20*, 325 – 331.
[40] G. Cornilescu, F. Delaglio, A. Bax, *J. Biomol. NMR* **1999**, *13*, 289 – 302.
[41] Y. Ishii, T. Terao, M. Kainosho, *Chem. Phys. Lett.* **1996**, *256*, 133 – 140.
[42] B. Reif, M. Hohwy, C. P. Jaroniec, C. M. Rienstra, R. G. Griffin, *J. Magn. Reson.* **2000**, *145*, 132 – 141.
[43] C. M. Rienstra, M. Hohwy, L. J. Mueller, C. P. Jaroniec, B. Reif, R. G. Griffin, *J. Am. Chem. Soc.* **2002**, *124*, 11908 – 11922.
[44] M. Hong, J. D. Gross, R. G. Griffin, *J. Phys. Chem. B* **1997**, *101*, 5869 – 5874.
[45] P. R. Costa, J. D. Gross, M. Hong, R. G. Griffin, *Chem. Phys. Lett.* **1997**, *280*, 95 – 103; X. Feng, P. J. E. Verdegem, Y. K. Lee, D. Sandstrom, M. Eden, P. BoveeGeurts, W. J. deGrip, J. Lugtenburg, H. J. M. de Groot, M. H. Levitt, *J. Am. Chem. Soc.* **1997**, *119*, 6853 – 6857.
[46] F. J. Blanco, R. Tycko, *J. Magn. Reson.* **2001**, *149*, 131 – 138.
[47] V. Ladizhansky, C. P. Jaroniec, A. Diehl, H. Oschkinat, R. G. Griffin, *J. Am. Chem. Soc.* **2003**, *125*, 6827 – 6833.
[48] T. A. Cross, M. H. Frey, S. J. Opella, *J. Am. Chem. Soc.* **1983**, *105*, 7471 – 7473.
[49] F. Castellani, B. J. van Rossum, A. Diehl, K. Rehbein, H. Oschkinat, *Biochemistry* **2003**, *42*, 11476 – 11483; B. J. van Rossum, F. Castellani, J. Pauli, K. Rehbein, J. Hollander, H. J. M. de Groot, H. Oschkinat, *J. Biomol. NMR* **2003**, *25*, 217 – 223.
[50] D. Suter, R. R. Ernst, *Phys. Rev. B* **1982**, *25*, 6038 – 6041; D. Suter, R. R. Ernst, *Phys. Rev. B* **1985**, *32*, 5608 – 5627; A. Kubo, C. A. McDowell, *J. Chem. Soc. Faraday Trans. I* **1988**, *84*, 3713 – 3730.
[51] K. Wüthrich, *NMR of Proteins and Nucleic Acids*, Wiley Interscience, New York, **1986**.
[52] H. Heise, K. Seidel, M. Etzkorn, S. Becker, M. Baldus, *J. Magn. Reson.* **2005**, *173*, 64 – 74.
[53] P. Guntert, *Prog. Nucl. Magn. Reson. Spectrosc.* **2003**, *43*, 105 – 125.
[54] M. Nilges, M. J. Macias, S. I. Odonoghue, H. Oschkinat, *J. Mol. Biol.* **1997**, *269*, 408 – 422.
[55] A. J. Wand, J. L. Urbauer, R. P. McEvoy, R. Bieber, *J. Biochem.* **1996**, *35*, 6116 – 6125.
[56] A. C. Wang, S. Grzesiek, R. Tschudin, P. J. Lodi, A. Bax, *J. Biomol. NMR* **1995**, *5*, 376 – 382.
[57] N. Tjandra, A. Szabo, A. Bax, *J. Am. Chem. Soc.* **1996**, *118*, 6986 – 6991.
[58] G. A. Lazar, J. R. Desjarlais, T. M. Handel, *Protein Sci.* **1997**, *6*, 1167 – 1178; J. You, R. E. Cohen, C. M. Pickart, *BioTechniques* **1999**, *27*, 950 – 954.
[59] S. R. Hartmann, E. L. Hahn, *Phys. Rev.* **1962**, *128*, 2042 – 2053.
[60] G. Metz, X. L. Wu, S. O. Smith, *J. Magn. Reson. Ser. A* **1994**, *110*, 219 – 227.
[61] A. E. Bennett, C. M. Rienstra, M. Auger, K. V. Lakshmi, R. G. Griffin, *J. Chem. Phys.* **1995**, *103*, 6951 – 6958.
[62] B. M. Fung, A. K. Khitrin, K. Ermolaev, *J. Magn. Reson.* **2000**, *142*, 97 – 101.
[63] S. Vijaykumar, C. E. Bugg, W. J. Cook, *J. Mol. Biol.* **1987**, *194*, 531 – 544.
[64] A. T. Brunger, P. D. Adams, G. M. Clore, W. L. DeLano, P. Gros, R. W. Grosse-Kunstleve, J. S. Jiang, J. Kuszewski, M. Nilges, N. S. Pannu, R. J. Read, L. M. Rice, T. Simonson, G. L. Warren, *Acta Crystallogr. Sect. D Biol. Crystallogr.* **1998**, *54*, 905 – 921.
[65] M. Nilges, *Curr. Opin. Struct. Biol.* **1996**, *6*, 617 – 623.
[66] R. Koradi, M. Billeter, K. Wüthrich, *J. Mol. Graphics* **1996**, *14*, 51 – 60.

Received: February 28, 2005
Published online on August 11, 2005

